

Polarisation measurements of five pulsars with interpulses

M. J. Keith^{1*}, S. Johnston¹, P. Weltevrede¹ and M. Kramer^{2,3}

¹ *Australia Telescope National Facility, CSIRO, P.O. Box 76, Epping, NSW 1710, Australia*

² *Max-Planck-Institut für Radioastronomie, Auf dem Hügel 69, 53121 Bonn, Germany*

³ *University of Manchester, Jodrell Bank Centre for Astrophysics, Alan Turing Building, Manchester M13 9PL, UK*

ABSTRACT

We present polarisation observations of five pulsars whose profiles exhibit two distinct emission regions separated by close to 180° of longitude. We fitted the position angle of the linear polarisation using the rotating vector model and convincingly show that all the pulsars have the angle between their magnetic and rotation axes close to 90°. The simplest interpretation of the results is that we see ‘main pulse’ emission from one pole and ‘interpulse’ emission from the opposite pole. We have attempted to produce emission maps of the magnetosphere above the polar caps for each pulsar and find that the maps support the view that the emission region in pulsars is complex, even when the profile appears simple. For three pulsars, we can derive emission heights and polar maps which are consistent with emission regions located symmetrically about the magnetic axis and confined to the open field lines. For two pulsars, we find that either the emission arises from ‘closed’ field lines or that the profiles are highly asymmetric with respect to the magnetic axis.

Key words: pulsars: general

1 INTRODUCTION

The measured width of pulsar profiles is typically less than 10 percent of the pulse period. Exceptions to this rule exist and can broadly be classified into three types (Weltevrede & Johnston 2008a). In the first type, which we refer to as interpulse pulsars, the profile has two distinct regions of emissions separated by close to 180°. The interpretation is that we see emission from open field lines near the two magnetic poles of the pulsar when the magnetic and rotation axes are orthogonal. In the second type, emission occurs over a large fraction of the pulse period; these are generally thought to be pulsars in which the magnetic and rotation axes are close to alignment. Finally, in younger pulsars, wide double profiles are observed the interpretation of which is that either the height from which the radio emission originates is rather large (Johnston & Weisberg 2006; Karastergiou & Johnston 2007) or the emission arises in a fan-beam (Manchester 1996).

An alternative physical model for the interpulse pulsars suggests that emission from both the main pulse (MP) and interpulse (IP) actually originate from the same magnetic pole (Dyks et al. 2005). In this model, the MP is seen as normal emission as the axis crosses close to the line of sight, and the IP is seen as ‘inward’ emission from the same pole as it crosses directly opposite to the line of sight.

For this paper, we carried out polarisation observations of a selection of five pulsars with strong IP emission, and applied the rotating vector model (RVM; Radhakrishnan & Cooke 1969) to determine their geometry. PSR J0627+0706 was discovered in the Perseus Arm pulsar survey (as yet unpublished). The other four pulsars, PSRs J1549–4848, J1722–3712, J1739–2903 and J1828–1101, are previously discovered (Manchester et al. 1996, 1978; Clifton & Lyne 1986; Morris et al. 2002), but have little or no published polarisation data. We describe the observations and the method used to fit RVM in Section 2 and discuss how to construct polar maps in Section 3. In Section 4 we present polarisation profiles and derive emission heights for each pulsar in turn. In Section 5 we discuss the implications of these results and provide a short conclusion in Section 6.

2 OBSERVATIONS AND RVM FITS

The five pulsars were observed using the Parkes 64-m radio telescope with data recorded using a digital spectrometer. Each pulsar was observed at 1.4 GHz with an integration time sufficient to yield a high signal-to-noise ratio. PSR J1828–1101 is heavily scattered at 1.4 GHz; we therefore observed it at 3.1 GHz. For details of the observing setup and calibration procedure, readers should refer to Johnston et al. (2008) and Weltevrede & Johnston (2008a).

* Email: mkeith@pulsarastronomy.net

Table 1. Parameters for seven pulsars from fits to the RVM.

Name	α_{MP}	β_{MP}	α_{IP}	β_{IP}	ϕ_0	$\Delta\phi_{\text{I}}$	$\Delta\phi_{\text{PA}}$	OG
J0627+0706	86.0 ± 0.2	8.7 ± 0.3	94.0 ± 0.3	0.7 ± 0.1	94.8 ± 0.2	176.2	179.4 ± 0.4	MP
J0908-4913	96.1 ± 0.4	-5.9 ± 0.6	83.9 ± 0.2	6.3 ± 0.4	96.42 ± 0.07	184.5	179.99 ± 0.06	IP
B1055-52	75.2 ± 0.4	36.1 ± 0.6	104.8 ± 0.4	6.1 ± 0.6	137.4 ± 0.6	204	189.5 ± 1.3	MP
J1549-4848	92.5 ± 0.2	-3.5 ± 0.2	87.5 ± 0.2	1.5 ± 0.2	93.0 ± 0.2	180	183.4 ± 0.3	MP
J1722-3712	90.7 ± 0.1	5.4 ± 0.3	89.3 ± 0.1	6.7 ± 0.5	95.0 ± 0.1	179.7	181.5 ± 1.2	IP
J1739-2903	84.2 ± 0.3	3.3 ± 0.2	95.8 ± 0.2	-8.2 ± 0.4	88.1 ± 0.1	180.7	182.7 ± 0.7	IP
J1828-1101	97.31 ± 0.6	-10.6 ± 1.5	82.7 ± 0.6	4.0 ± 1.4	94.8 ± 0.7	180.2	178 ± 6	MP

Table 2. Parameters for seven pulsars used to derive their polar maps.

Name	Period (s)	MP		IP		R_{LC} (km)	r_{em} (km)	$\Delta\phi$ (deg)
		$(\phi_1 - \phi_0)$	$(\phi_{\text{t}} - \phi_0)$	$(\phi_1 - \phi_0)$	$(\phi_{\text{t}} - \phi_0)$			
J0627+0706	0.47588	-6.6	1.4	-10.0	6.9	22700	160/320	1.6/3.2
J0908-4913	0.10675	-16.5	3.5	-19	0	5100	245	11
B1055-52	0.19711	-15	22	-42	10	9400	730	18
J1549-4848	0.28835	-11.5	7	-11.5	4	13700	180	2.9
J1722-3712	0.23617	-17	5	-13.5	1	11300	290	6.0
J1739-2903	0.32288	-8.1	9.9	-9.1	9.9	15400	45/230	0.7/3.4
J1828-1101	0.07205	-11.3	4.2	-10.8	3.2	3400	55	3.5

The RVM shows that the characteristic S-shaped swing of the polarisation position angle (PA) can be explained if the PA of the linear polarisation (LP) is defined by the direction of the magnetic field at the point of emission (Radhakrishnan & Cooke 1969). If one assumes that the polarised emission is well modelled by the RVM, then one can use polarisation measurements to constrain the geometry. The geometry of a pulsar is characterised by two parameters, α , the angle between the magnetic and rotation axes, and β , the minimum angle between the magnetic axis and the line of sight to the observer. The RVM also allows derivation of two other parameters, ϕ_0 which is the pulse longitude at which the PA swing has the steepest gradient, and Ψ_0 which is the PA at that longitude. In this paper we adopt the convention that the angle between the rotation axis and the line of sight to the observer, $\zeta = \alpha + \beta$. The RVM states that the observed PA, Ψ , depends on the pulse longitude, ϕ , and the geometric parameters as

$$\tan(\Psi + \Psi_0) = \frac{\sin \alpha \sin(\phi - \phi_0)}{\sin \zeta \cos \alpha - \cos \zeta \sin \alpha \cos(\phi - \phi_0)}. \quad (1)$$

We follow the ‘RVM sign convention’ for the PA (see Everett & Weisberg 2001).

For the majority of pulsars, the range of pulse longitude for which the PA can be measured (i.e. the range where there is significant emission) is small. When this is the case, the RVM fit for α and β is highly degenerate and it is difficult to constrain the geometry. However, in the case of pulsars with an IP, we can usually measure the PA in two, well-separated, regions of pulse longitude and therefore break this degeneracy. Although Weltevrede & Johnston (2008b) tabulated a list of 27 pulsars, which they considered to be an upper limit to the number of orthogonal rotators in the observed population, only the recent result on PSR J0908-4913 by Kramer & Johnston (2008) shows incontrovertible evidence for this directly from RVM fits. This is partly because the PA swings of many pulsars deviate from purely geometrical values due to effects both in the pulsar magnetosphere (e.g. orthogonal mode emission; Karastergiou et al. 2002) and in

the interstellar medium (e.g. scattering effects; Karastergiou 2009).

The RVM was fitted to the PA swing for the five pulsars in our sample using a non-linear ordinary least-squares algorithm. Table 1 gives the results for the five pulsars and for PSRs J0908-4913 and B1055-52 for which high signal-to-noise data have been presented elsewhere (Kramer & Johnston 2008; Weltevrede & Wright 2009). In addition to the geometric parameters, we also present the separation of the steepest gradient in the MP and IP, $\Delta\phi_{\text{PA}}$. This is computed by fitting independent values of ϕ_0 for the PAs of the MP and IP. All five parameters are then fitted simultaneously.

The confidence contours shown in later figures and the standard errors in Table 1 have been generated by scaling the observed PA errors so that $\chi^2 = 1$. These errors assume that the RVM model can fully describe the observed PA swing. It is clear however that the residuals have small but significant unmodeled variability, and the errors we present are likely to underestimate the true error in the model parameters.

2.1 Implications for gamma-ray emission

The *Fermi* satellite has recently detected a large number of gamma-ray pulsars (Abdo et al. 2009). The implication of the detections is that gamma-ray emission arises in the outer magnetosphere. In the so-called ‘outer-gap’ model (Cheng et al. 1986; Romani 1996), gamma-rays are only observed from field lines above the null charge line. For pulsars in which both radio and gamma-ray emission are detected, the gamma-ray emission is associated with the opposite magnetic pole to the radio emission. However, in the case of orthogonal rotators in which radio emission is seen from both poles, knowledge of α and β allows us to determine whether the MP or the IP emission originates from above the same pole as any putative gamma-ray emission. This is listed in the final column of Table 1. Of our sample, only PSR B1055-52 has been detected in gamma-rays to

date but on-going *Fermi* observations may uncover further detections.

3 EMISSION HEIGHT AND POLAR MAPS

For emission which originates from the neutron star surface, ϕ_0 corresponds to the point where the magnetic axis passes closest to the line of sight. If the emission height, r_{em} , is small with respect to the light-cylinder radius, R_{LC} , then the steepest gradient of the PA swing arrives later with respect to the corresponding total intensity emission. The relative shift between the intensity of the emission and ϕ_0 is given by

$$\Delta\phi = 4r_{\text{em}}/R_{\text{LC}} \quad (2)$$

(Blaskiewicz et al. 1991; Hibschan & Arons 2001; Dyks 2008). The phase offset, $\Delta\phi$, is often measured by assuming a fiducial point on the profile which is either the profile peak or the symmetry centre (see e.g. Blaskiewicz et al. 1991; Johnston & Weisberg 2006). This method has its difficulties because the choice of fiducial point is somewhat subjective. If one assumes the emission height is the same for both MP and IP, then one expects that $\Delta\phi_{\text{PA}} = 180^\circ$ (see Table 1). Table 1 also lists $\Delta\phi_{\text{I}}$, the separation between the MP and IP in total intensity. This is estimated by choosing an suitable fiducial point for both the MP and IP of each pulsar, nominally the centre of the pulse.

Recently, Weltevrede & Wright (2009) have shown how to identify the active regions of the polar cap given the observational data and an assumption about the emission height. First they define a parameter, s , the distance between the footpoint of the active field line and the magnetic axis divided by the polar cap radius. The field lines at the magnetic axis therefore have $s = 0$ and the last open field lines have $s = 1$. The observational data consist of the difference in longitude of the leading (ϕ_{l}) and trailing (ϕ_{t}) edges of the profile with respect to ϕ_0 . These values for both the MP and IP for each pulsar are listed in columns 3 and 4 of Table 2. Generally, the location of ϕ_0 is closer to the trailing edge than the leading edge. This is expected from Equation 2, if the assumption is made that the profile is intrinsically symmetric. Indeed, Blaskiewicz et al. (1991) used this assumption to derive emission heights in a range of pulsars.

Although the symmetry argument is appealing, it may not be correct, especially if the emission is patchy across the beam (Lyne & Manchester 1988). Weltevrede & Wright (2009) derived a formalism which allows s to be computed as a function of emission height and we use their methodology to produce such a figure for each pulsar in our sample. Then, by choosing an emission height we can produce a map showing the emission regions above the polar cap. What criteria should govern our choice of emission height? We pick two possible examples. The first enables us to obtain a symmetric solution, that is, one where the s value is the same for the leading and trailing edges of the profile. The second is to obtain a solution where $s < 1$ so that the emission arises from the open field lines of the polar cap. In the standard picture one might expect both these conditions to be met simultaneously. For two of the pulsars in our sample we find that this is not the case. All the pulsars are considered in detail below.

4 DISCUSSION OF INDIVIDUAL PULSARS

4.1 PSR J0627+0706 (Figure 1)

The RVM fit shows that this pulsar is an orthogonal rotator. The line of sight passes less than $\sim 1^\circ$ from the magnetic axis corresponding to the IP emission, with the MP passing further from the axis with $\beta \sim 9^\circ$. The peak of the MP occurs 5° earlier than ϕ_0 .

At 0.7 GHz the MP consists of steep rising edge followed by a smoother trailing edge. At 1.4 GHz a second component can be discerned in the trailing part of the profile which becomes more prominent at 3.1 GHz. The MP has an overall width of $\sim 12^\circ$. The LP is modest at all frequencies and there is some negative circular polarisation (CP). The PA swing is smooth with no sign of orthogonal mode jumps.

The IP is broader than the MP with a width of some 20° , as might be expected given $|\beta_{\text{IP}}| < |\beta_{\text{MP}}|$. The IP amplitude is around 20% of the MP and its spectral index is steeper. The profile consists of a smooth rising and trailing edge and is double peaked, with the two peaks separated by $\sim 4^\circ$. The LP is rather low and there is some negative CP. The PA swing is steep through the centre of the profile and there is an orthogonal jump prior to the first pulse peak.

One interpretation of the profile is that the MP is a ‘partial profile’ (e.g. Lyne & Manchester 1988) where the leading edge of the beam is seen, but the trailing edge is absent. As can be seen in Figure 1(c), there are two choices of r_{em} that yield symmetric solutions. The first solution with $r_{\text{em}} = 0.007R_{\text{LC}} = 160$ km, (see Figure 1(d)) causes the IP to neatly fill the open field line region, however the MP emission then occurs well outside the open field line region. The second solution with $r_{\text{em}} = 0.014R_{\text{LC}} = 320$ km, (see Figure 1(e)) places the MP symmetrically inside the open field line region, but now the IP is displaced towards the trailing edge of the beam. There is no emission height which allows both the MP and IP to be symmetrically located.

4.2 PSR J1549–4848 (Figure 2)

The RVM fit shows the pulsar to be an orthogonal rotator with the line of sight cutting close to both magnetic axes. For this pulsar it appears that the separation between the steepest gradients of the PA for MP and IP is 3° away from the expected 180° . However, we argue that the similarity in width between the MP and IP, combined with their similar β values and the lack of an apparent shift in $\Delta\phi_{\text{I}}$ strongly suggests that the emission height is the same for both the MP and IP, and the fitting is affected by unmodeled perturbations in the observed PA.

At 1.4 GHz the MP has a width of $\sim 20^\circ$ and the profile is lopsided, possibly consisting of 3 blended components. The LP is moderate, reaching a peak near the centre of the profile. The PA swing is smooth and unbroken. At 0.7 GHz the leading component of the profile is weaker than at 1.4 GHz whereas at 3.1 GHz it is stronger. The RVM fit shows that the line of sight crosses the magnetic axis very close to the peak of the profile.

The IP is somewhat narrower than the MP with a width of some $\sim 15^\circ$ at 1.4 GHz. Its amplitude is about 30% that of the MP, this rises with increasing frequency and so the IP has a shallower spectral index than the MP. Its profile

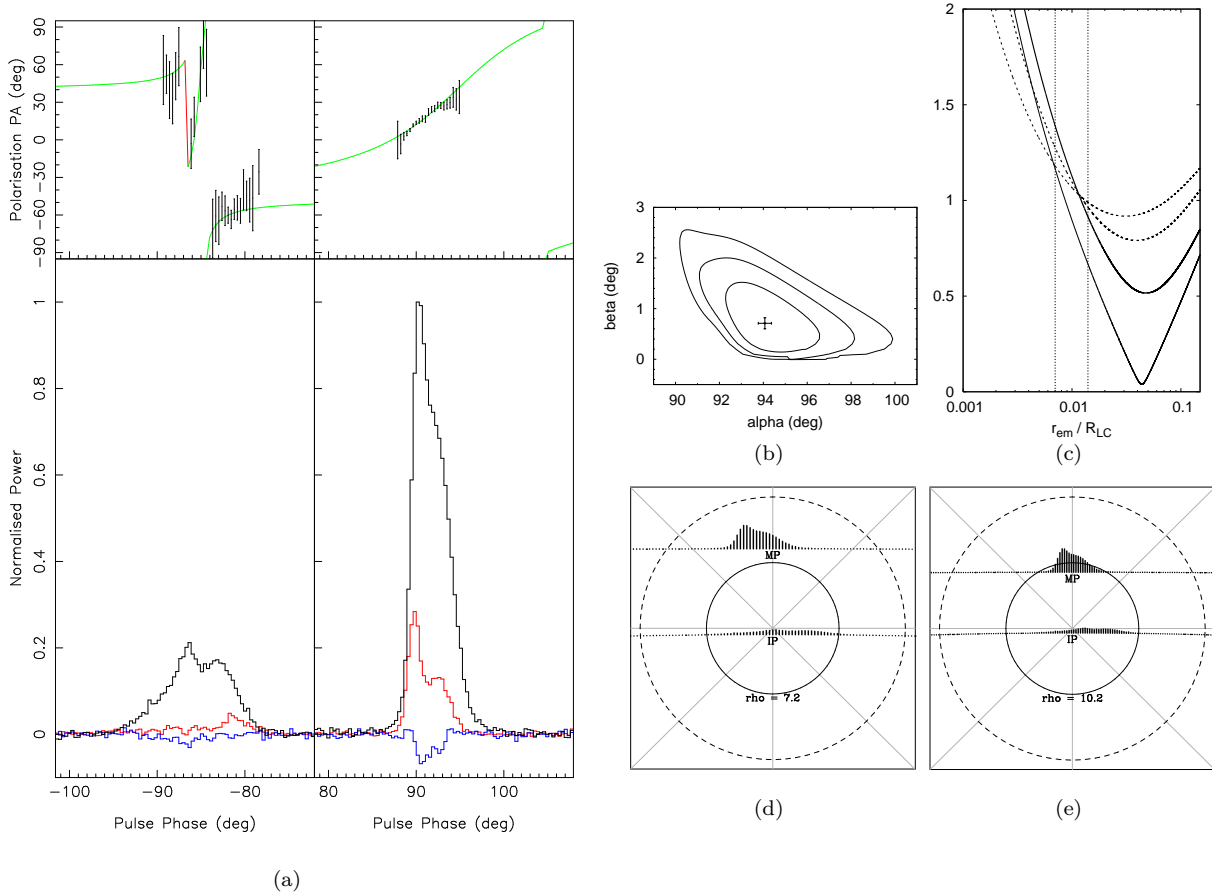


Figure 1. (a) The 1.4 GHz integrated profile of PSR J0627+0706 near $\phi = \pm 90^\circ$. The peak flux density has been placed at a longitude of 90° . The lower part of the figure shows the total intensity (black), LP (red) and CP (blue). The upper part of the figure shows the measured PA and the RVM fit. An orthogonal jump can be seen near phase -88° . (b) Contours of constant χ^2 in the residuals of the RVM fit as a function of α and β . The contours approximate 1,2 and 3- σ confidence limits. The cross marks the position of the minimum χ^2 . (c) s values for the leading (solid lines) and trailing (dashed lines) edge of the MP (thick lines) and IP (thin lines) as a function of r_{em} . The vertical lines show choices of r_{em} used for Figures (d) and (e). (d) and (e) polar cap emission maps for $r_{\text{em}} = 160$ and 320 km respectively. The MP and IP have been mapped onto the geometric model, with the IP reflected horizontally so that field lines are physically identical for both MP and IP. The inner circle denotes the extent of the open field line region, $s = 1$, and the outer circle is twice this extent.

appear to be a triple structure with high LP through the pulse centre. The PA traverse is broken by an orthogonal jump between the central and trailing components.

Our choice of emission height, $0.013R_{\text{LC}} = 180$ km, gives a symmetric solution, with the open field line region nearly filled for both the MP and IP (see Figure 2(d)).

4.3 PSR J1722–3712 (Figure 3)

The RVM fit shows that the pulsar is an almost perfectly orthogonal rotator, with the line of sight cutting some 6° away from the magnetic axis for both the MP and IP. The peak of the profile leads ϕ_0 by $\sim 5^\circ$.

The MP has an overall width of $\sim 20^\circ$ and the profile shows some evolution with frequency but is reasonably symmetrical over the range considered here. At 0.7 GHz the profile has a steep trailing edge, this resolves into a small trailing component at 1.4 GHz which is more prominent again at 3.1 GHz. The LP fraction is $\sim 40\%$ at all three frequencies

and there is significant positive CP. The PA swing is smooth and unbroken with no sign of orthogonal mode jumps.

The IP in this pulsar is rather weak, less than 10% of the MP amplitude. This makes it hard to discern any structure or any trend with frequency but it appears to be double peaked and virtually 100% linearly polarised.

We choose an emission height of $0.026R_{\text{LC}} = 290$ km which places the centroid of emission for both MP and IP coincident with the magnetic axis. The polar cap map (Figure 3(d)) shows that the open field line region is more-or-less filled with emission.

4.4 PSR J1739–2903 (Figure 4)

The RVM fit constrains the magnetic and rotation axes to be within 5 to 10° of orthogonality. The RVM fit shows that the magnetic axis crossing occurs almost exactly in the profile centre.

The MP undergoes significant evolution with frequency. The MP width at 0.7 GHz is $\sim 17^\circ$, whereas at 1.4 and

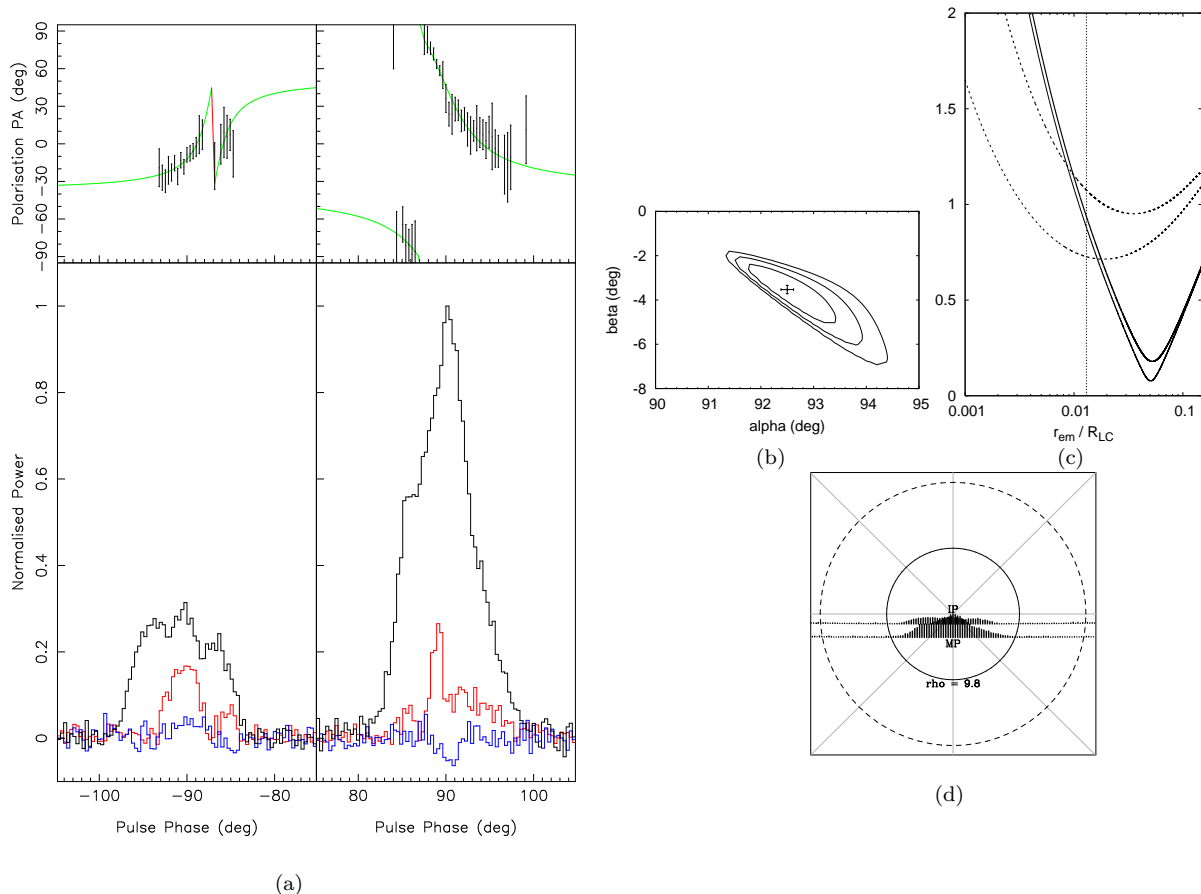


Figure 2. (a) The 1.4 GHz integrated pulse profile of PSR J1549–4848, clipped to show the details of the two pulses. An orthogonal jump can be seen near phase of -87° . The format of this plot, and the others in this figure are the same as for Figure 1. The polar cap emission map in (d) assumes $r_{em} = 180$ km.

3.1 GHz the width is more like $\sim 10^\circ$. It is possible that the low frequency profile is affected by scatter broadening. At 1.4 and 3.1 GHz the profile is split into two narrower, blended components. The trailing component is brighter than the leading component at 1.4 GHz but the reverse is true at 3.1 GHz. The LP and CP fractions are very low. There is a hint that the CP changes from negative to positive in the pulse centre at 1.4 GHz.

The IP is relatively strong in this pulsar, with an amplitude of about 40% of the MP at 0.7 and 1.4 GHz and 25% at 3.1 GHz. The separation of the centroid of the MP and IP is almost exactly 180° . The profile width is $\sim 15^\circ$ at all frequencies. At 1.4 GHz the profile consists of an asymmetric single component and there is little evolution with frequency. The IP is relatively highly linearly polarised and has negative CP. The PA swing is unbroken across the pulse.

It is rather difficult to choose a sensible emission height for this pulsar. There are no solutions for which the emission lies entirely within the open field line region. From Figure 4(c), we have chosen two emission heights, one with a symmetrical solution, and the second that forces the bulk of the emission to lie within the open field line region. The first height, $r_{em} = 0.003R_{LC} = 45$ km, (see Figure 4(d)) shows the components symmetrically located about the magnetic axis. However the IP emission then comes from a location twice the radius of the polar cap, as does the outer edges of

the MP. The second solution, $r_{em} = 0.015R_{LC} = 230$ km, (see Figure 4(e)) is the best attempt at locating the emission within the open field line regions, however both MP and IP are significantly displaced towards the trailing edge of the beam.

4.5 PSR J1828–1101 (Figure 5)

We find that no satisfactory RVM fit can be obtained without the addition of an orthogonal mode jump between the MP and IP and, in this case, the RVM fit yields an orthogonal geometry. The centroid of emission of the MP lags ϕ_0 by approximately 2° .

PSR J1828–1101 is highly scattered at 1.4 GHz and not detectable at 0.7 GHz. We therefore describe and show the 3.1 GHz profile. The MP at 3.1 GHz consists of a single component with a total width of $\sim 10^\circ$. The LP fraction is about 50% and there is a smooth swing of PA across the pulse. The CP is low. The IP, which is about 20% the amplitude of the MP lies almost exactly 180° from the MP. The profile consists of a single component of width $\sim 14^\circ$ and appears to be highly linearly polarised with significant negative CP. The PA swing is smooth across the profile.

We choose an emission height of $0.016R_{LC} = 55$ km, which gives both a symmetric solution for the MP and IP and ensures that $s < 1$ (see Figure 5(c)).

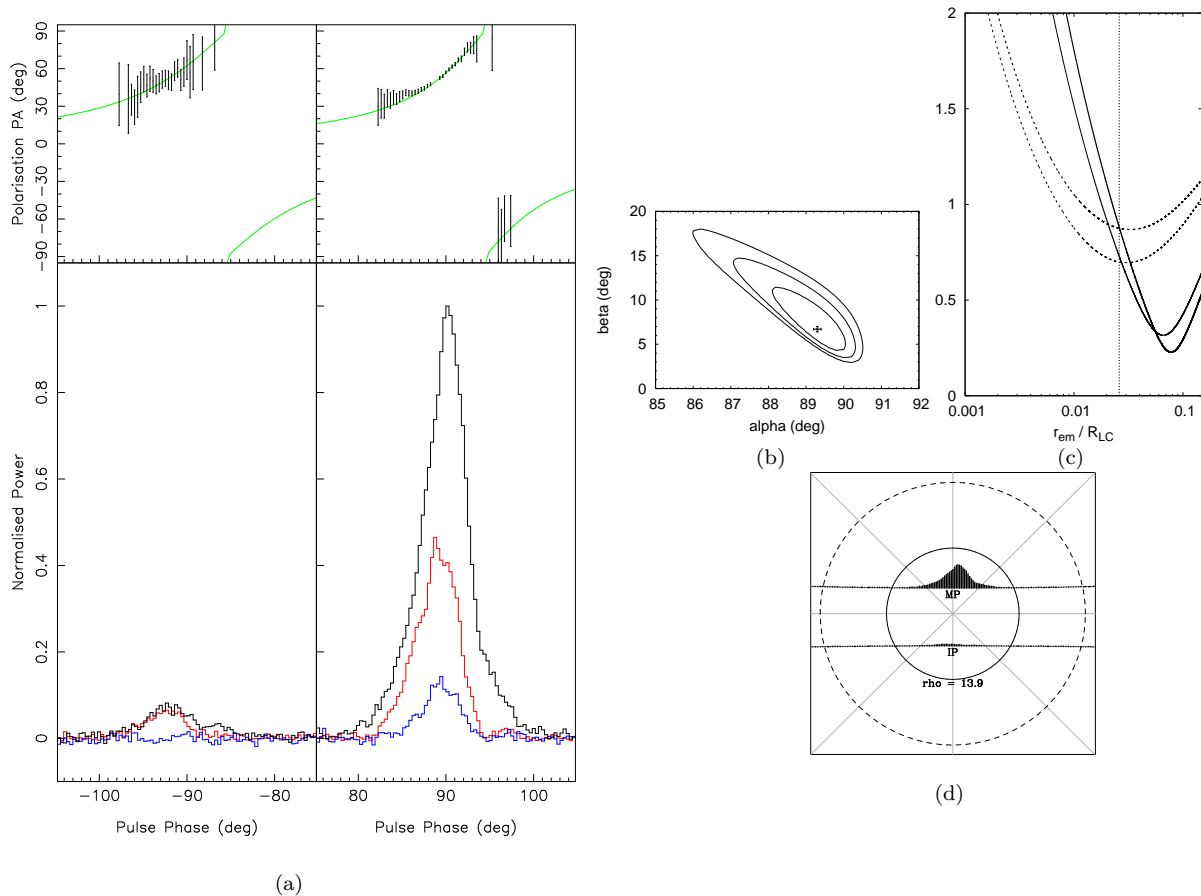


Figure 3. (a) The 1.4 GHz integrated pulse profile of PSR J1722–3712, clipped to show the details of the two pulses. The format of this plot, and the others in this figure are the same as for Figure 1. The polar cap emission map in (d) assumes $r_{\text{em}} = 290$ km.

5 DISCUSSION

5.1 Orthogonal rotator statistics

If the α distribution in pulsars is random, then one would expect $\sim 5\%$ of pulsars to have IP emission. The actual fraction is lower than this: Weltevrede & Johnston (2008b) listed only 27 pulsars with IP emission out of a total of nearly 1500 objects. The discovery of PSR J0627+0706 since then raises the number to 28. Remarkably, at the time of that paper, there was no firm evidence that *any* of these 27 pulsars had $\alpha \sim 90^\circ$. There is a variety of explanations for this: RVM fits are not possible in pulsars where the LP is very low, where the IP is very weak, or where the PAs are distorted from their geometrical expectations. The list also contains several ‘notorious’ pulsars (PSRs B0950+08, B1702–19, B1822–09 and B1929+10) where RVM fits cannot distinguish between orthogonal and aligned rotators (see e.g. Everett & Weisberg 2001 and references therein). PSRs B1702–19 and B1822–09 are particularly interesting because the single pulse data seem to show evidence that the MP and IP somehow communicate information (Weltevrede et al. 2007; Gil et al. 1994).

We have convincingly shown that the five pulsars in this paper have PA swings which yield $\alpha \approx 90^\circ$. In addition, the recent results on PSRs B0906–49 (Kramer & Johnston 2008) and B1055–52 (Weltevrede & Wright 2009) now demonstrate that at least seven pulsars are orthogonal rota-

tors. A single pulse study of these IP pulsars is warranted in light of the data on PSRs B1702–19 and B1822–09. The results for these pulsars strongly support the ‘standard’ model where the MP and IP are emission from corresponding poles of the pulsar but, in the next section consider the possibility of inwards emission.

5.2 Inward emission model

An alternative to the standard view of observing emission from both poles is a model where emission is seen both outward and inward from an emission zone above a single magnetic pole (Dyks et al. 2005). In this model, the standard outward emission makes up one component of the profile and the inward emission, from the same pole, is seen $\sim 180^\circ$ later. With a dipole field the inward emission originates from the same field lines that would be active in the forward emission from the other pole. This makes it difficult to observationally distinguish the two cases. Because the inward emission arises from the other side of the star, there is a delay in arrival which allows the separation of the peaks to exceed 180° .

If IP pulsars are associated with inwards emission from a single pole, we would expect that $\Delta\phi_{\text{PA}} - 180^\circ = 180^\circ - \Delta\phi_{\text{I}}$, which follows from the fact that the intensity and PA swing are shifted in opposite directions to the outwards case (Dyks et al. 2005). For four of the pulsars in our sample,

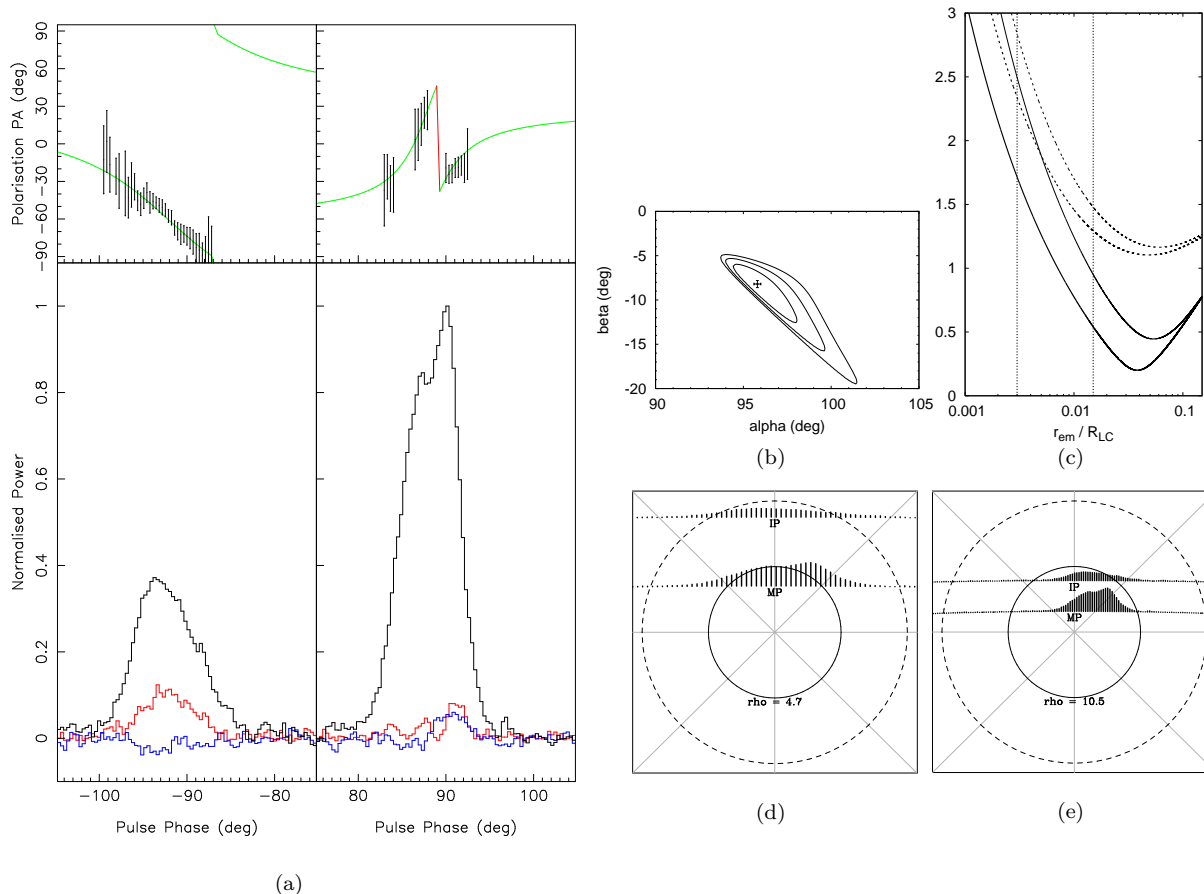


Figure 4. (a) The 1.4 GHz integrated pulse profile of PSR J1739–2903, clipped to show the details of the two pulses. An orthogonal jump can be seen around a phase of 89° . The format of this plot, and the others in this figure are the same as for Figure 1. The polar cap emission map in (d) assumes $r_{\text{em}} = 45$ km and in (e) assumes $r_{\text{em}} = 230$ km.

both $\Delta\phi_I$ and $\Delta\phi_{\text{PA}}$ are close to 180° and no firm conclusions can be drawn. However, for PSRs J0627+0706, J0908–4913 and B1055–52 the offset from 180° in the observed intensity cannot be explained by inwards emission and we believe this model can be ruled out with some certainty.

5.3 Active field line regions

We have shown that the emission heights above both magnetic poles are rather similar for a given pulsar (except perhaps for PSR J1549–4848). If this is the case, one might expect that the profiles should be wider for small values of β than for large values. However, the profile widths of the MP and IP are rather similar even when the difference in β is large. It is also clear that the observed profile luminosity also does not depend on β in the way one would expect for a smoothly filled emission region. Therefore these data support the view that the shape of the emission region in pulsars is complex, even when the observed profile appears simple.

Apart from PSR B1055–52, the emission heights we derive are low, with values of a few hundred km, or only $\sim 1\%$ of the light cylinder radius (see Table 2). For PSRs J0908–4913, J1549–4848, J1722–3712 and J1828–1101 we obtain a satisfactory solution to the emission height which yields symmetry of the profiles around the magnetic axis

and emission located well within the open field line region. For PSR J0627+0706 we find that either the IP is symmetrically located about the magnetic axis in which case the MP has emission from outside the open field lines, or the MP lies within the open field lines and the IP is located on the far trailing edge of the polar cap. For PSR J1739–2903 the situation is more problematic. In this case, a symmetrical solution gives emission from outside the open field lines for both the MP and IP. Forcing the emission into the open field lines means both MP and IP are significantly displaced to the trailing part of the beam. Weltevrede & Wright (2009) found for PSR B1055–52 that there is no choice of emission height for which the emission comes from entirely within the open field line region.

6 CONCLUSION

Analysis of the PA swings of five pulsars with IP emission shows that they can be well fitted with the RVM. Although it is clear that there are small perturbations on top of the simple geometric model, the five pulsars discussed in this paper plus PSRs J0908–4913 (Kramer & Johnston 2008) and B1055–52 (Weltevrede & Wright 2009) show convincing evidence that their magnetic and spin axis are close to orthogonal.

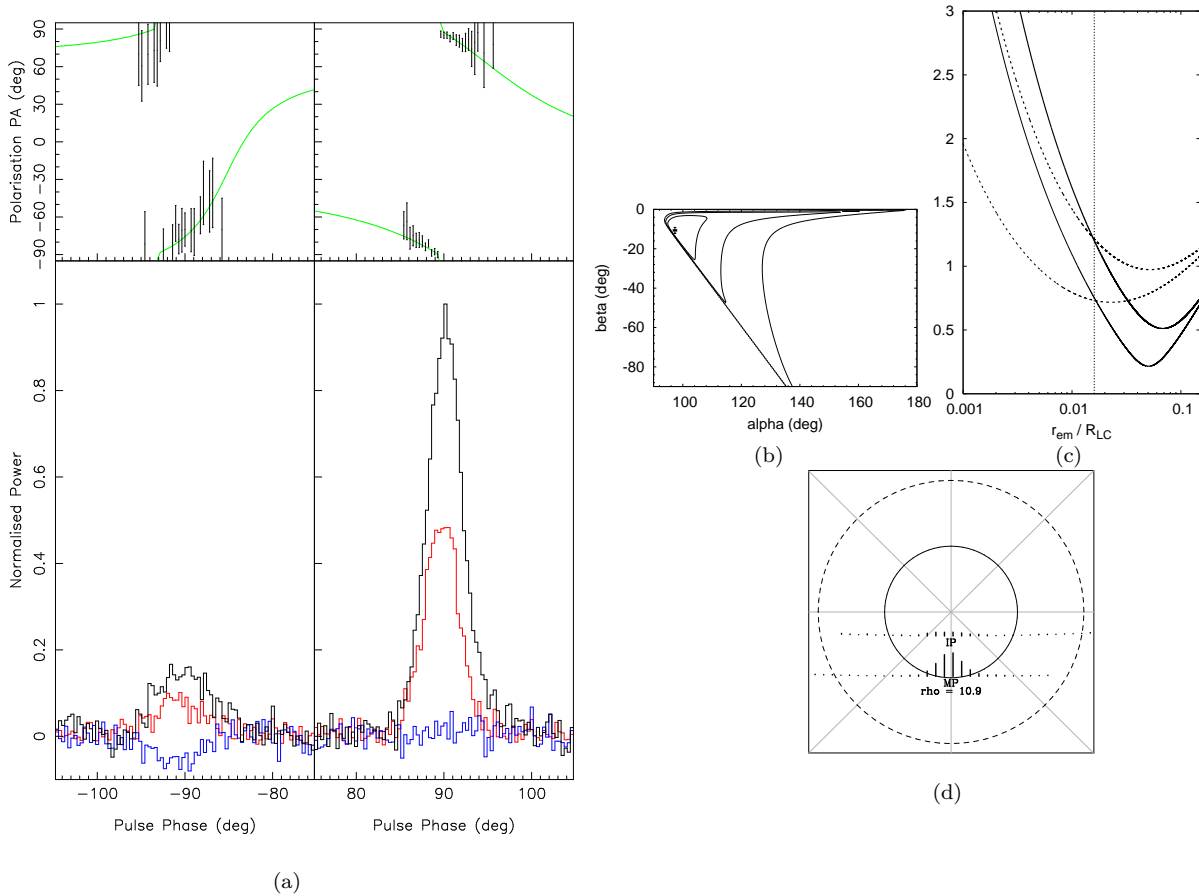


Figure 5. (a) The 3.1 GHz integrated pulse profile of PSR J1828–1101, clipped to show the details of the two pulses. Note that there is an orthogonal mode jump between the MP and IP. The format of this plot, and the others in this figure are the same as for Figure 1. The polar cap emission map in (d) assumes $r_{em} = 55$ km.

We use a technique developed in Weltevrede & Wright (2009) in order to map the emission regions the polar cap in each pulsar. General conclusions which can be drawn are that the emission appears to be patchy and does not conform to a uniform conal illumination and that the emission height is similar at the two poles for a given pulsar. We find that for three of our pulsars, emission maps can be made which show both symmetry about the magnetic axis and emission confined to the open field lines. In two cases, however, we find that either emission arises from ‘closed’ field lines or that the profiles are highly asymmetric with respect to the magnetic pole.

REFERENCES

- Abdo A. A. et al., 2009, ApJS, Submitted
 Blaskiewicz M., Cordes J. M., Wasserman I., 1991, ApJ, 370, 643
 Cheng K. S., Ho C., Ruderman M., 1986, ApJ, 300, 500
 Clifton T. R., Lyne A. G., 1986, Nature, 320, 43
 Dyks J., 2008, MNRAS, 391, 859
 Dyks J., Zhang B., Gil J., 2005, ApJ, 626, L45
 Everett J. E., Weisberg J. M., 2001, ApJ, 553, 341
 Gil J. A. et al., 1994, A&A, 282, 45
 Hibschan J. A., Arons J., 2001, ApJ, 546, 382
 Johnston S., Karastergiou A., Mitra D., Gupta Y., 2008, MNRAS, 388, 261
 Johnston S., Weisberg J. M., 2006, MNRAS, 368, 1856
 Karastergiou A., 2009, MNRAS, 392, L60
 Karastergiou A., Johnston S., 2007, MNRAS, 380, 1678
 Karastergiou A., Kramer M., Johnston S., Lyne A. G., Bhat N. D. R., Gupta Y., 2002, A&A, 391, 247
 Kramer M., Johnston S., 2008, MNRAS, 390, 87
 Lyne A. G., Manchester R. N., 1988, MNRAS, 234, 477
 Manchester R. N., 1996, in Johnston S., Walker M. A., Bailes M., ed, Pulsars: Problems and Progress, IAU Colloquium 160. Astronomical Society of the Pacific, San Francisco, p. 193
 Manchester R. N. et al., 1996, MNRAS, 279, 1235
 Manchester R. N., Lyne A. G., Taylor J. H., Durdin J. M., Large M. I., Little A. G., 1978, MNRAS, 185, 409
 Morris D. J. et al., 2002, MNRAS, 335, 275
 Radhakrishnan V., Cooke D. J., 1969, Astrophys. Lett., 3, 225
 Romani R. W., 1996, ApJ, 470, 469
 Weltevrede P., Johnston S., 2008a, MNRAS, 391, 1210
 Weltevrede P., Johnston S., 2008b, MNRAS, 387, 1755
 Weltevrede P., Wright G., 2009, MNRAS, 395, 2117
 Weltevrede P., Wright G. A. E., Stappers B. W., 2007, A&A, 467, 1163